Quark model study of the η photo-production:

Evidence for a new S_{11} resonance?

B. Saghai[1,a] and Z. Li[2]

[1] Service de Physique Nucléaire, DAPNIA - CEA/Saclay, F-91191 Gif-sur-Yvette Cedex, France
[2] Physics Department, Peking University, Beijing 100871, P.R. China

Abstract. An extensive and systematic study of the recent η photo-production data up to 1.2 GeV is presented within a chiral constituent quark model. A model embodying all known nucleonic resonances shows clear need for a yet undiscovered third S_{11} resonance in the second resonance region, for which we determine the mass (1.729 GeV) and the total width (183 MeV). Furthermore, we extract the configuration mixing angles, an important property of the quark-quark interaction in the quark model, for the resonances $S_{11}(1535)$ and $S_{11}(1650)$, as well as for the resonances $D_{13}(1520)$ and $D_{13}(1700)$. Our results agree well with the quark model predictions. In addition, the partial ηN decay widths and/or the photo-excitation helicity amplitudes for the nucleonic resonances $S_{11}(1535)$, $S_{11}(1650)$, $P_{11}(1710)$, $P_{13}(1720)$, $D_{13}(1520)$, $D_{13}(1700)$, $D_{15}(1675)$, and $F_{15}(1680)$ are also obtained in this approach.

PACS. 12.39.Fe Chiral Lagrangians – 13.40.Hq Electromagnetic decays – 13.60.Le Meson production – 14.20.Gk Baryon resonances with $S = 0$

1 Introduction

Investigation of the η-meson production via electromagnetic probes offers access to several exciting topics in hadron spectroscopy.

One prominent example is the search for missing resonances. Several such baryons have been predicted by different QCD inspired approaches and constitute a strong test of these formalisms[1]. Electromagnetic production of such resonances, if they exist, is looked for in various mesons production processes. To our knowledge, the most extensive theoretical results in the quark model approach have been reported in ref. [5], where the authors, within a relativized pair creation ($^3P_0$) model, have investigated the quasi–two-body decays of baryons and have proceeded to make comparisons with the available results from partial-wave analysis [6,7].

Another example, more specific to the ηN final state, is the enhancement [8–12] of the resonance $S_{11}(1535)$ decaying into the ηN and the suppression of another S-wave resonance $S_{11}(1650)$ in the same channel, which provide us with direct insights into the configuration mixings of the quark model states. A recent work [13], embodying the fine-structure interaction between constituent quarks, has provided a qualitative description of the suppressed decay

of the $S_{11}(1650) \rightarrow N\eta$ compared to the large branching ratio for the $S_{11}(1535) \rightarrow N\eta$ decay, though the electromagnetic couplings of the resonance $S_{11}(1535)$ remain to be evaluated in this approach. It has also been suggested [14] that quasi-bound $K\Lambda$ or $K\Sigma$ states might be an answer to this puzzle.

Moreover, the properties of the decay of baryon resonances into γN and/or meson-nucleon are intimately related to their internal structure [5,15–18]. Extensive recent experimental efforts on the η photo- [19–24] and electroproduction [25,26] are opening a new era in this topic. The process $\gamma p \rightarrow \eta p$, with real or virtual photons, has been proven [27–34] to be very attractive in the extraction of the photo-excitation amplitudes of the $S_{11}(1535)$ and/or $D_{13}(1520)$ resonances. Perhaps more importantly, the data make it possible to improve the accuracy in the determination of the $N^* \rightarrow \eta N$ branching ratios.

All these features can be studied through the η-meson photo-production. At the present time, the near threshold region has been studied extensively via a variety of formalisms, such as effective Lagrangian approaches [29–36], generalized Lee model [37], coupled-channel calculations [38–41], chiral meson-baryon Lagrangian theory [42–44], and constituent quark formalism [27,45–48].

These efforts have considerably improved our understanding of the underlying elementary reaction mechanism at low energy. Here, the most quantitative phenomenological investigations concern the first resonance region, where

---

[a] e-mail: `bsaghai@cea.fr`
[1] See, *e.g.*, review papers [1–4], and references therein.

the differential and total cross-section data obtained at Mainz [20], for $E_\gamma^{\rm lab} < 0.8$ GeV have been extensively exploited. Some of those works include also target polarization asymmetry form ELSA [21], and/or polarized beam asymmetry from Graal [22]. The main finding on the reaction mechanism is the dominance of the $S_{11}(1535)$ resonance and a small contribution from the $D_{13}(1520)$ resonance. Moreover, these studies have concentrated on putting constraints on the $S_{11}(1535)$, and to a less extent on the $D_{13}(1520)$ resonances parameters.

Very recent differential and total cross-section data from Graal [23] cover both first and second resonance regions and constitute a real break-through in this field.

The focus of this paper is to study all the recent $\gamma p \to \eta p$ data for $E_\gamma^{\rm lab} < 1.2$ GeV ($W \equiv E_{\rm total}^{\rm cm} < 1.75$ GeV) within a chiral constituent quark formalism based on the $SU(6) \otimes O(3)$ symmetry. The advantage of the quark model for the meson photo-production is the ability to relate the photo-production data directly to the internal structure of the baryon resonances. To go beyond the exact $SU(6) \otimes O(3)$ symmetry, we introduce symmetry breaking coefficients C_{N^*} as in our earlier publication [27]. We further show how these coefficients are related to the configuration mixing angles generated by the gluon exchange interactions in the quark model [49,50]. Indeed, our extracted mixing angles for the S- and D-wave resonances in the second resonance region show very good agreement with the quark model predictions [49].

Our main finding in the present work is *the need for a third S_{11} resonance in the second resonance region*, as seemingly dictated by the Graal cross-section data [23] above $E_\gamma^{\rm lab} \approx 1.0$ GeV. Such a resonance has been predicted by the authors of ref. [14]. Our extracted values for the mass and width of this resonance agree very well with those put forward in that paper. If this is confirmed by more accurate and/or higher-energy data, then one possible conclusion would be that this resonance cannot be accommodated by the constituent quark model, indicating a molecular type of structure [14].

In addition, we present a framework for extracting the ηN branching ratios from the data beyond the resonances in the threshold region of the η photo-production.

This paper is organized as follows. In the next section, we summarize the theoretical basis of our work, introduce the configuration mixing angles and relate them to the $SU(6) \otimes O(3)$ symmetry breaking coefficients. We present also expressions for photo-excitation helicity amplitudes and strong decay widths. Section 3 is devoted to our numerical results. We start with comparisons between our results and differential cross-section data. Results for mixing angles are given and the need for a new resonance is underlined. Then we proceed to comparisons with total cross-section and polarization observables and show the role played by the third S_{11} resonance. The obtained model is then used to extract the helicity amplitudes and strong decay widths. In sect. 4 we summarize our work and end it with some concluding remarks.

2 Theoretical frame

The starting point of the meson photo-production in the chiral quark model is the low-energy QCD Lagrangian [51]

$$\mathcal{L} = \bar{\psi} \left[\gamma_\mu (i\partial^\mu + V^\mu + \gamma_5 A^\mu) - m \right] \psi + \dots , \qquad (1)$$

where ψ is the quark field in the $SU(3)$ symmetry, $V^\mu = (\xi^\dagger \partial_\mu \xi + \xi \partial_\mu \xi^\dagger)/2$ and $A^\mu = i(\xi^\dagger \partial_\mu \xi - \xi \partial_\mu \xi^\dagger)/2$ are the vector and axial currents, respectively, with $\xi = e^{i\Pi f}$; f is a decay constant and the field Π is a $3 \otimes 3$ matrix

$$\Pi = \begin{vmatrix} \frac{1}{\sqrt{2}}\pi^0 + \frac{1}{\sqrt{6}}\eta & \pi^+ & K^+ \\ \pi^- & -\frac{1}{\sqrt{2}}\pi^0 + \frac{1}{\sqrt{6}}\eta & K^0 \\ K^- & \bar{K}^0 & -\sqrt{\frac{2}{3}}\eta \end{vmatrix}, \qquad (2)$$

in which the pseudoscalar mesons, π, K, and η, are treated as Goldstone bosons so that the Lagrangian in eq. (1) is invariant under the chiral transformation. Therefore, there are four components for the photo-production of pseudoscalar mesons based on the QCD Lagrangian

$$\mathcal{M}_{fi} = \langle N_{\rm f} | H_{m,e} | N_{\rm i} \rangle$$

$$+ \sum_j \left\{ \frac{\langle N_{\rm f} | H_m | N_j \rangle \langle N_j | H_e | N_{\rm i} \rangle}{E_{\rm i} + \omega - E_j} \right.$$

$$\left. + \frac{\langle N_{\rm f} | H_e | N_j \rangle \langle N_j | H_m | N_{\rm i} \rangle}{E_{\rm i} - \omega_m - E_j} \right\} + \mathcal{M}_T , \qquad (3)$$

where $N_{\rm i}(N_{\rm f})$ is the initial (final) state of the nucleon, and $\omega(\omega_m)$ represents the energy of incoming (outgoing) photons (mesons).

The first term in eq. (3) is a seagull term. It is generated by the gauge transformation of the axial vector A_μ in the QCD Lagrangian. This term, being proportional to the electric charge of the outgoing mesons, does not contribute to the production of the η-meson. The second and third terms correspond to the s- and u-channels, respectively. The last term is the t-channel contribution and contains two parts: i) charged meson exchanges which are proportional to the charge of outgoing mesons and thus do not contribute to the process $\gamma N \to \eta N$; ii) ρ and ω exchange in the η production which are excluded here due to the duality hypothesis [52,53]. We will come back to this point in sect. 4.

The pseudovector and electromagnetic couplings at the tree level are given, respectively, by the following standard expressions:

$$H_m = \sum_j \frac{1}{f_m} \bar{\psi}_j \gamma_\mu^j \gamma_5^j \psi_j \partial^\mu \phi_m, \qquad (4)$$

$$H_e = -\sum_j e_j \gamma_\mu^j A^\mu(\mathbf{k}, \mathbf{r}). \qquad (5)$$

Because the baryon resonances in the s- and u-channels are treated as three-quark systems, the separation of the center-of-mass motion from the internal motions in the transition operators is crucial. Thus, we use a well-established approach [54] to evaluate the contributions from resonances in the s- and u-channels.

2.1 Configuration mixing

The general framework for the meson photo-production, in particular, for the η case, has been given in refs. [45,46]. The transition matrix elements based on the low-energy QCD Lagrangian include the s- and u-channel contributions

$$\mathcal{M}_{if} = \mathcal{M}_s + \mathcal{M}_u. \tag{6}$$

The u-channel contributions are divided into the nucleon Born term and the contributions from the excited resonances. The matrix elements for the nucleon Born term is given explicitly, while the contributions from the excited resonances above 2 GeV for a given parity are assumed to be degenerate so that their contributions could be written in a compact form [45].

The contributions from the s-channel resonances can be written as

$$\mathcal{M}_{N^*} = \frac{2M_{N^*}}{s - M_{N^*}(M_{N^*} - i\Gamma(q))} e^{-\frac{k^2 + q^2}{6\alpha_{\text{ho}}^2}} \mathcal{A}_{N^*}, \tag{7}$$

where $k = |\mathbf{k}|$ and $q = |\mathbf{q}|$ represent the momenta of the incoming photon and the outgoing meson respectively, $\sqrt{s}$ is the total energy of the system, $e^{-(k^2+q^2)/6\alpha_{\text{ho}}^2}$ is a form factor in the harmonic oscillator basis with the parameter α_{ho}^2 related to the harmonic oscillator strength in the wave function, and M_{N^*} and $\Gamma(q)$ are the mass and the total width of the resonance, respectively. The amplitudes $\mathcal{A}_{N^*}$ are divided into two parts [45,46]: the contribution from each resonance below 2 GeV, the transition amplitudes of which have been translated into the standard CGLN amplitudes in the harmonic oscillator basis, and the contributions from the resonances above 2 GeV treated as degenerate, since little experimental information is available on those resonances.

The contributions from each resonance to the η photo-production is determined by introducing [27] a new set of parameters C_{N^*}, and the following substitution rule for the amplitudes $\mathcal{A}_{N^*}$:

$$\mathcal{A}_{N^*} \to C_{N^*} \mathcal{A}_{N^*}, \tag{8}$$

so that

$$\mathcal{M}_{N^*}^{\text{exp}} = C_{N^*}^2 \mathcal{M}_{N^*}^{\text{qm}}, \tag{9}$$

where $\mathcal{M}_{N^*}^{\text{exp}}$ is the experimental value of the observable, and $\mathcal{M}_{N^*}^{\text{qm}}$ is calculated in the quark model [46]. The $SU(6) \otimes O(3)$ symmetry predicts $C_{N^*} = 0.0$ for $S_{11}(1650)$, $D_{13}(1700)$, and $D_{15}(1675)$ resonances, and $C_{N^*} = 1.0$ for other resonances in table 1. Thus, the coefficients C_{N^*} measure the discrepancies between the theoretical results and the experimental data and show the extent to which the $SU(6) \otimes O(3)$ symmetry is broken in the process investigated here.

One of the main reasons that the $SU(6) \otimes O(3)$ symmetry is broken is due to the configuration mixings caused by the one-gluon exchange [50]. Here, the most relevant configuration mixings are those of the two S_{11} and the two D_{13} states around 1.5 to 1.7 GeV. The configuration mixings can be expressed in terms of the mixing angle between

Table 1. Resonances included in our study with their assignments in $SU(6) \otimes O(3)$ configurations, masses, and widths. The mass and width of the $S_{11}(1535)$ resonance are left as adjustable parameters (see table 4).

States	$SU(6) \otimes O(3)$	Mass (GeV)	Width (GeV)
$S_{11}(1535)$	$N(^2P_M)_{\frac{1}{2}-}$		
$S_{11}(1650)$	$N(^4P_M)_{\frac{1}{2}-}$	1.650	0.150
$D_{13}(1520)$	$N(^2P_M)_{\frac{3}{2}-}$	1.520	0.130
$D_{13}(1700)$	$N(^4P_M)_{\frac{3}{2}-}$	1.700	0.150
$D_{15}(1675)$	$N(^4P_M)_{\frac{5}{2}-}$	1.675	0.150
$P_{13}(1720)$	$N(^2D_S)_{\frac{3}{2}+}$	1.720	0.150
$F_{15}(1680)$	$N(^2D_S)_{\frac{5}{2}+}$	1.680	0.130
$P_{11}(1440)$	$N(^2S'_S)_{\frac{1}{2}+}$	1.440	0.150
$P_{11}(1710)$	$N(^2S_M)_{\frac{1}{2}+}$	1.710	0.100
$P_{13}(1900)$	$N(^2D_M)_{\frac{3}{2}+}$	1.900	0.500
$F_{15}(2000)$	$N(^2D_M)_{\frac{5}{2}+}$	2.000	0.490

the two $SU(6) \otimes O(3)$ states $|N(^2P_M)\rangle$ and $|N(^4P_M)\rangle$, with the total quark spin 1/2 and 3/2;

$$\begin{pmatrix} |S_{11}(1535)\rangle \\ |S_{11}(1650)\rangle \end{pmatrix} = \begin{pmatrix} \cos\theta_S & -\sin\theta_S \\ \sin\theta_S & \cos\theta_S \end{pmatrix} \begin{pmatrix} |N(^2P_M)_{\frac{1}{2}-}\rangle \\ |N(^4P_M)_{\frac{1}{2}-}\rangle \end{pmatrix}, \tag{10}$$

and

$$\begin{pmatrix} |D_{13}(1520)\rangle \\ |D_{13}(1700)\rangle \end{pmatrix} = \begin{pmatrix} \cos\theta_D & -\sin\theta_D \\ \sin\theta_D & \cos\theta_D \end{pmatrix} \begin{pmatrix} |N(^2P_M)_{\frac{3}{2}-}\rangle \\ |N(^4P_M)_{\frac{3}{2}-}\rangle \end{pmatrix}, \tag{11}$$

where the mixing angle θ is predicted to be $-32°$ for the S_{11} resonances and $6°$ for the D_{13} resonances in the Isgur-Karl Model [49].

To show how the coefficients C_{N^*} are related to the mixing angles, we express the amplitudes $\mathcal{A}_{N^*}$ in terms of the product of the photo and meson transition amplitudes

$$\mathcal{A}_{N^*} \propto \langle N|H_m|N^*\rangle\langle N^*|H_e|N\rangle, \tag{12}$$

where H_m and H_e are the meson and photon transition operators, respectively. Using eqs. (10) to (12), for the resonance $S_{11}(1535)$, one finds

$$\mathcal{A}_{S_{11}} \propto \langle N|H_m(\cos\theta_S|N(^2P_M)_{\frac{1}{2}-}\rangle - \sin\theta_S$$
$$\times |N(^4P_M)_{\frac{1}{2}-}\rangle)(\cos\theta_S\langle N(^2P_M)_{\frac{1}{2}-}|$$
$$- \sin\theta_S\langle N(^4P_M)_{\frac{1}{2}-}|)H_e|N\rangle, \tag{13}$$

Table 2. Electromagnetic helicity amplitudes for the γp within the present quark model, with E_γ the energy of the incoming photon, $m_q = 330$ MeV quark mass, and $e^{-\mathcal{K}^2/6\alpha_{\mathrm{ho}}^2}$ a form factor in the harmonic oscillator basis. Here $\mathcal{K} = (\frac{\sqrt{2s}M_N}{s+M_N^2})k$, with M_N the mass of the nucleon. As explained in the text, for the D_{15} the γn helicity amplitudes are given.

Resonance	$A_{1/2}^p$	$A_{3/2}^p$
S_{11}	$\dfrac{2\sqrt{2}}{3}\left(\dfrac{E_\gamma m_q}{\alpha_{\mathrm{ho}}^2} + \dfrac{1}{2}\dfrac{\mathcal{K}^2}{\alpha_{\mathrm{ho}}^2}\right)\sqrt{\dfrac{\pi}{E_\gamma}}\mu\alpha_{\mathrm{ho}}e^{-\frac{\mathcal{K}^2}{6\alpha_{\mathrm{ho}}^2}}$	
P_{11}	$-\dfrac{1}{3\sqrt{6}}\left(\dfrac{\mathcal{K}}{\alpha_{\mathrm{ho}}}\right)^2\sqrt{\dfrac{\pi}{E_\gamma}}\mu\mathcal{K}e^{-\frac{\mathcal{K}^2}{6\alpha_{\mathrm{ho}}^2}}$	
P_{13}	$\dfrac{2}{\sqrt{15}}\left(\dfrac{E_\gamma m_q}{\alpha_{\mathrm{ho}}^2} + \dfrac{1}{3}\dfrac{\mathcal{K}^2}{\alpha_{\mathrm{ho}}^2}\right)\sqrt{\dfrac{\pi}{E_\gamma}}\mu\mathcal{K}e^{-\frac{\mathcal{K}^2}{6\alpha_{\mathrm{ho}}^2}}$	$-\dfrac{2}{3\sqrt{5}}\dfrac{E_\gamma m_q}{\alpha_{\mathrm{ho}}^2}\sqrt{\dfrac{\pi}{E_\gamma}}\mu\mathcal{K}e^{-\frac{\mathcal{K}^2}{6\alpha_{\mathrm{ho}}^2}}$
D_{13}	$\dfrac{2}{3}\left(\dfrac{E_\gamma m_q}{\alpha_{\mathrm{ho}}^2} - \dfrac{\mathcal{K}^2}{\alpha_{\mathrm{ho}}^2}\right)\sqrt{\dfrac{\pi}{E_\gamma}}\mu\alpha_{\mathrm{ho}}e^{-\frac{\mathcal{K}^2}{6\alpha_{\mathrm{ho}}^2}}$	$\dfrac{2}{\sqrt{3}}\dfrac{E_\gamma m_q}{\alpha_{\mathrm{ho}}^2}\sqrt{\dfrac{\pi}{E_\gamma}}\mu\alpha_{\mathrm{ho}}e^{-\frac{\mathcal{K}^2}{6\alpha_{\mathrm{ho}}^2}}$
D_{15}	$\dfrac{-2}{3\sqrt{10}}\dfrac{\mathcal{K}^2}{\alpha_{\mathrm{ho}}^2}\sqrt{\dfrac{\pi}{E_\gamma}}\mu\alpha_{\mathrm{ho}}e^{-\frac{\mathcal{K}^2}{6\alpha_{\mathrm{ho}}^2}}$	$\dfrac{-2}{3\sqrt{5}}\dfrac{\mathcal{K}^2}{\alpha_{\mathrm{ho}}^2}\sqrt{\dfrac{\pi}{E_\gamma}}\mu\alpha_{\mathrm{ho}}e^{-\frac{\mathcal{K}^2}{6\alpha_{\mathrm{ho}}^2}}$
F_{15}	$\dfrac{2\sqrt{2}}{3\sqrt{5}}\left(\dfrac{E_\gamma m_q}{\alpha_{\mathrm{ho}}^2} - \dfrac{1}{2}\dfrac{\mathcal{K}^2}{\alpha_{\mathrm{ho}}^2}\right)\sqrt{\dfrac{\pi}{E_\gamma}}\mu\mathcal{K}e^{-\frac{\mathcal{K}^2}{6\alpha_{\mathrm{ho}}^2}}$	$\dfrac{4}{3\sqrt{5}}\dfrac{E_\gamma m_q}{\alpha_{\mathrm{ho}}^2}\sqrt{\dfrac{\pi}{E_\gamma}}\mu\mathcal{K}e^{-\frac{\mathcal{K}^2}{6\alpha_{\mathrm{ho}}^2}}$

Due to the Moorhouse selection rule [55], the photon transition amplitude $\langle N(^4P_M)_{\frac{1}{2}^-}|H_e|N\rangle$ vanishes [46] in our model. So, eq. (13) becomes

$$\mathcal{A}_{S_{11}} \propto (\cos^2\theta_S - \mathcal{R}\sin\theta_S\cos\theta_S)\langle N|H_m|N(^2P_M)_{\frac{1}{2}^-}\rangle$$
$$\times\langle N(^2P_M)_{\frac{1}{2}^-}|H_e|N\rangle, \tag{14}$$

where $\langle N|H_m|N(^2P_M)_{\frac{1}{2}^-}\rangle\langle N(^2P_M)_{\frac{1}{2}^-}|H_e|N\rangle$ determines [46] the CGLN amplitude for the $|N(^2P_M)_{\frac{1}{2}^-}\rangle$ state, and the ratio

$$\mathcal{R} = \frac{\langle N|H_m|N(^4P_M)_{\frac{1}{2}^-}\rangle}{\langle N|H_m|N(^2P_M)_{\frac{1}{2}^-}\rangle} \tag{15}$$

is a constant determined by the $SU(6)\otimes O(3)$ symmetry. Using the the meson transition operator H_m from the Lagrangian used in deriving the CGLN amplitudes in the quark model, we find $\mathcal{R} = -1$ for the S_{11} resonances and $\sqrt{1/10}$ for the D_{13} resonances. Then, the configuration mixing coefficient can be related to the configuration mixing angles

$$C_{S_{11}(1535)} = \cos\theta_S(\cos\theta_S - \sin\theta_S), \tag{16}$$

$$C_{S_{11}(1650)} = -\sin\theta_S(\cos\theta_S + \sin\theta_S), \tag{17}$$

$$C_{D_{13}(1520)} = \cos\theta_D(\cos\theta_D - \sqrt{1/10}\sin\theta_D), \tag{18}$$

$$C_{D_{13}(1700)} = \sin\theta_D(\sqrt{1/10}\cos\theta_D + \sin\theta_D). \tag{19}$$

2.2 Photo-excitation helicity amplitudes and ηN decay width of baryon resonances

The total cross-section in the η photo-production for a given resonance can be expressed as

$$\sigma \propto \Gamma_{\eta N}(A_{1/2}^2 + A_{3/2}^2). \tag{20}$$

In the quark model, the helicity amplitudes $(A_{1/2})_{\mathrm{qm}}$ and $(A_{3/2})_{\mathrm{qm}}$ and the partial width $\Gamma_{\eta N}^{\mathrm{qm}}$ are *calculated explicitly* (tables 2 and 3).

Then the above configuration mixing coefficients C_{N^*} are introduced and their numerical values are extracted by fitting the experimental data, so that

$$\sigma \propto \Gamma_{\eta N}^{\mathrm{th}}(A_{1/2}^2 + A_{3/2}^2)_{\mathrm{qm}}, \tag{21}$$

where

$$\Gamma_{\eta N}^{\mathrm{th}} \equiv C_{N^*}^2\Gamma_{\eta N}^{\mathrm{qm}}. \tag{22}$$

The purpose of the procedure developed here is to extract the experimental value of the partial width $\Gamma_{\eta N}^{\mathrm{exp}}$ in

$$\sigma \propto \Gamma_{\eta N}^{\mathrm{exp}}(A_{1/2}^2 + A_{3/2}^2)_{\mathrm{exp}}, \tag{23}$$

if the helicity amplitude is well defined from other sources, or to determine the helicity amplitde if the partial width is well known from other sources. Then from eqs. (21) to (23),

$$\Gamma_{\eta N}^{\mathrm{exp}} = C_{N^*}^2\Gamma_{\eta N}^{\mathrm{qm}}\frac{(A_{1/2}^2 + A_{3/2}^2)_{\mathrm{qm}}}{(A_{1/2}^2 + A_{3/2}^2)_{\mathrm{exp}}}. \tag{24}$$

As mentioned above, the quantities $\Gamma_{\eta N}^{\mathrm{qm}}$, $(A_{1/2})_{\mathrm{qm}}$ and $(A_{3/2})_{\mathrm{qm}}$ in eq. (24) can be explicitly calculated in the quark model, and consistency requires that the Lagrangian used in evaluating these quantities must be the

Table 3. Expressions for the ηN decay widths of the resonances, with $\mathcal{Q} = (\frac{M_N}{E_{\mathrm{f}}})q$, and E_{f} the energy of the final state nucleon.

Resonance	$\Gamma_{\eta N}^{\mathrm{qm}}$
S_{11}	$\dfrac{4}{9}\alpha_{\eta NN}\dfrac{E_{\mathrm{f}}}{M_{N^*}}\dfrac{\mathcal{Q}}{M_N^2}\left[\dfrac{M_{N^*}+M_N}{E_{\mathrm{f}}+M_N}\dfrac{\mathcal{Q}^2}{\alpha_{\mathrm{ho}}}-\dfrac{3}{2}\dfrac{E_\eta}{m_q}\right]^2 e^{-\frac{\mathcal{Q}^2}{3\alpha_{\mathrm{ho}}^2}}$
P_{11}	$\dfrac{2}{3}\alpha_{\eta NN}\dfrac{E_{\mathrm{f}}}{M_{N^*}}\dfrac{\mathcal{Q}}{M_N^2}\left[\dfrac{M_{N^*}+M_N}{E_{\mathrm{f}}+M_N}\dfrac{\mathcal{Q}^3}{\alpha_{\mathrm{ho}}^2}-\dfrac{E_\eta\mathcal{Q}}{m_q}\right]^2 e^{-\frac{\mathcal{Q}^2}{3\alpha_{\mathrm{ho}}^2}}$
P_{13}	$\dfrac{1}{15}\alpha_{\eta NN}\dfrac{E_{\mathrm{f}}}{M_{N^*}}\dfrac{\mathcal{Q}}{M_N^2}\left[\dfrac{M_{N^*}+M_N}{E_{\mathrm{f}}+M_N}\dfrac{\mathcal{Q}^3}{\alpha_{\mathrm{ho}}^2}-\dfrac{5}{2}\dfrac{E_\eta\mathcal{Q}}{m_q}\right]^2 e^{-\frac{\mathcal{Q}^2}{3\alpha_{\mathrm{ho}}^2}}$
D_{13}	$\dfrac{4}{9}\alpha_{\eta NN}\dfrac{E_{\mathrm{f}}}{M_{N^*}}\dfrac{\mathcal{Q}}{M_N^2}\left[\dfrac{M_{N^*}+M_N}{E_{\mathrm{f}}+M_N}\dfrac{\mathcal{Q}^2}{\alpha_{\mathrm{ho}}}\right]^2 e^{-\frac{\mathcal{Q}^2}{3\alpha_{\mathrm{ho}}^2}}$
D_{15}	$\dfrac{4}{15}\alpha_{\eta NN}\dfrac{E_{\mathrm{f}}}{M_{N^*}}\dfrac{\mathcal{Q}}{M_N^2}\left[\dfrac{M_{N^*}+M_N}{E_{\mathrm{f}}+M_N}\dfrac{\mathcal{Q}^2}{\alpha_{\mathrm{ho}}}\right]^2 e^{-\frac{\mathcal{Q}^2}{3\alpha_{\mathrm{ho}}^2}}$
F_{15}	$\dfrac{1}{15}\alpha_{\eta NN}\dfrac{E_{\mathrm{f}}}{M_{N^*}}\dfrac{\mathcal{Q}}{M_N^2}\left[\dfrac{M_{N^*}+M_N}{E_{\mathrm{f}}+M_N}\dfrac{\mathcal{Q}^3}{\alpha_{\mathrm{ho}}^2}\right]^2 e^{-\frac{\mathcal{Q}^2}{3\alpha_{\mathrm{ho}}^2}}$

same as that in deriving the CGLN amplitudes for each resonance [46]. The resulting photon vertex from the Lagrangian used in deriving the CGLN amplitudes is slightly different from those used in the previous calculations [15, 17]. As we will show later, this does not lead to significant changes in the numerical results. The derivation of the helicity amplitudes is standard, and we give them in table 2 for the process $N^* \to \gamma p$.

We would like to underline that the present quark model approach within the $SU(6) \otimes O(3)$ symmetry limit, predicts vanishing values for the γp photo-decay amplitudes for the resonances $D_{13}(1700)$ and $D_{15}(1675)$. In our previous work [27], in order to investigate possible deviations from this symmetry, we used the same expressions for the $D_{13}(1700)$ resonance as for the $D_{13}(1520)$ due to the configuration mixing effects. In the case of the resonance $D_{15}(1675)$, the configuration mixing effect is very small since there is only one D_{15} configuration in this mass region. Thus, for this latter resonance, the helicity amplitudes presented in table 2 correspond to the CGLN amplitudes for the $\gamma n \to \eta n$-channel, which was discussed in more detail in our previous study [27]. In this work, we have adopted the same procedure.

Finally, the formula derived within our quark model approach for the resonance decaying into the ηN are summarized in table 3. Here also we have consistently used the same Lagrangian as that in deriving the CGLN amplitudes in ref. [46].

3 Results and discussion

In this section, we compare the results of the quark model presented above, with the recent data [20–24].

3.1 Fitting procedure and extracted parameters

As mentioned above, within the exact $SU(6) \otimes O(3)$ symmetry scheme, the only free parameters of our approach are: the strength of the harmonic oscillator α_{ho} and the ηNN coupling constant $\alpha_{\eta NN} \equiv 2g_{\eta NN}$. However, introducing the symmetry breaking effects via the C_{N^*} coefficients (eq. (9)), we need in addition one free parameter per resonance. Given recent results from Graal [23] and JLab [25,26], we leave also as free parameters the mass and the width of the dominant $S_{11}(1535)$ resonance.

In this section, we report on three models summarized in table 4 and described below:

a) Model A: This model includes all the eleven known relevant resonances (table 1) with mass below 2 GeV, and hence contains 14 free parameters. Note that the strength of the Roper resonance is kept at its quark model value $C_{P11(1440)} = 1$, as discussed in ref. [27].

b) Model B: Here we introduce the mixing angle constraints, eqs. (16) to (19), as explained in sect. 2.1. So, the two strengths for the $S_{11}(1535)$ and $S_{11}(1650)$ resonances are replaced by the mixing angle θ_S. This is also the case for the resonances $D_{13}(1520)$ and $D_{13}(1700)$ related by the mixing angle θ_D. The number of free parameters is then reduced to 12.

c) Model C: In the presence of the mixing angle constraints as above, and for the reasons that will be explained in sect. 3.2, we introduce a third $S11$ resonance with three free parameters; namely, its mass, width, and strength. The number of free parameters increases to 15.

The free parameters of all the above three models have been extracted (table 4) using the MINUIT minimization code [56] from the CERN Library. The fitted data base contains 400 values: differential cross-sections from

Table 4. Free parameters and their extracted values; masses and widths are given in GeV.

Parameter	Model A	Model B	Model C
α_{ho}^2 (GeV^2)	0.090 ± 0.001	0.090 ± 0.001	0.090 ± 0.007
$\alpha_{\eta NN} \equiv 2g_{\eta NN}$	0.898 ± 0.012	1.530 ± 0.015	1.467 ± 0.020
Mass of $S_{11}(1535)$	1.530 ± 0.001	1.530 ± 0.001	1.542 ± 0.001
Width of $S_{11}(1535)$	0.140 ± 0.001	0.142 ± 0.001	0.162 ± 0.001
$C_{S_{11}(1535)}$	1.500 ± 0.001	1.167 ± 0.009	1.120 ± 0.003
$C_{S_{11}(1650)}$	-0.182 ± 0.011	-0.167 ± 0.009	-0.200 ± 0.003
θ_S	-	$-32.2° \pm 1.8°$	$-26.6° \pm 0.8°$
Mass of the third S_{11}	-	-	1.729 ± 0.003
Width of the third S_{11}	-	-	0.183 ± 0.010
Strength of the third S_{11}	-	-	0.542 ± 0.053
$C_{D_{13}(1520)}$	1.500 ± 0.014	0.964 ± 0.002	0.964 ± 0.002
$C_{D_{13}(1700)}$	0.100 ± 0.005	0.036 ± 0.002	0.036 ± 0.002
θ_D	-	$5.1° \pm 0.2°$	$5.1° \pm 0.2°$
$C_{P_{11}(1710)}$	1.790 ± 0.385	-0.837 ± 0.449	-1.057 ± 0.206
$C_{P_{13}(1720)}$	0.053 ± 0.052	0.305 ± 0.058	1.000 ± 0.010
$C_{P_{13}(1900)}$	-2.500 ± 0.030	-2.500 ± 0.013	-2.478 ± 0.047
$C_{F_{15}(1688)}$	0.814 ± 0.241	0.761 ± 0.202	2.123 ± 0.102
$C_{F_{15}(2000)}$	-2.500 ± 0.028	-2.500 ± 0.026	0.201 ± 0.426
$C_{D_{15}(1675}$	-0.505 ± 0.030	-0.382 ± 0.022	-0.169 ± 0.024
$\chi^2_{\mathrm{d.o.f.}}$	3.2	3.8	1.6

Mainz [20] and Graal [23], and the beam asymmetry polarization data from Graal [22].

In the following, we compare the results of our models with different fitted observables, but also with predicted ones, namely, total cross-section and the polarized target asymmetry.

3.2 Differential cross-section

The recent and accurate data for the differential cross-sections come from two groups and have been included in the fitted data base.

i) Mainz data [20]: Angular distributions, $\theta_\eta^{\mathrm{cm}} \approx 26°$ to $154°$, have been reported between $E_\gamma^{\mathrm{lab}} = 0.716$ GeV and 0.790 GeV at 10 energies. This data base contains 100 data points.

ii) Graal data [23]: Here, the angular distributions, $\theta_\eta^{\mathrm{cm}} \approx 20°$ to $160°$, have been measured between $E_\gamma^{\mathrm{lab}} = 0.714$ GeV and 1.1 GeV at 24 energies. This data base contains 225 data points. This set of data has larger uncertainties than the Mainz data, but goes well above the first resonance region.

Between the two above data sets, there are four overlapping energies. Here, to keep the number of the figures

reasonable, we show comparisons at twelve energies. In fig. 1, data and our results are shown between 0.732 GeV and 0.965 GeV, where there are three overlapping energies between Mainz and Graal data. At the two lowest energies, the three models A, B, and C reproduce equally well these data. At two intermediate energies as well as at the highest one, model C turns out to be superior to models A and B.

In Figure 2, results from 1.0 to 1.1 GeV are depicted. With increasing energy, the forward angle data are reproduced correctly only by model C, while above 1.06 GeV they are badly reproduced by models A and B. Before proceeding to comparisons with other observables, we discuss these three models in more detail.

Model A: Here the strengths of all relevant resonances are left as free parameters. This is the most simple-minded procedure in the sense that the $SU(6) \otimes O(3)$ symmetry breaking is introduced, allowing contributions from the three resonances $S_{11}(1650)$, $D_{13}(1700)$, and $D_{15}(1675)$, without any constraint from the mixing angle relations (eqs. (16) to (19)).

This approach was already applied in a previous paper [27], to a more restricted data base. One of the main interests here is to find out by how much the strengths of those three resonances deviate from zero, which is the pre-
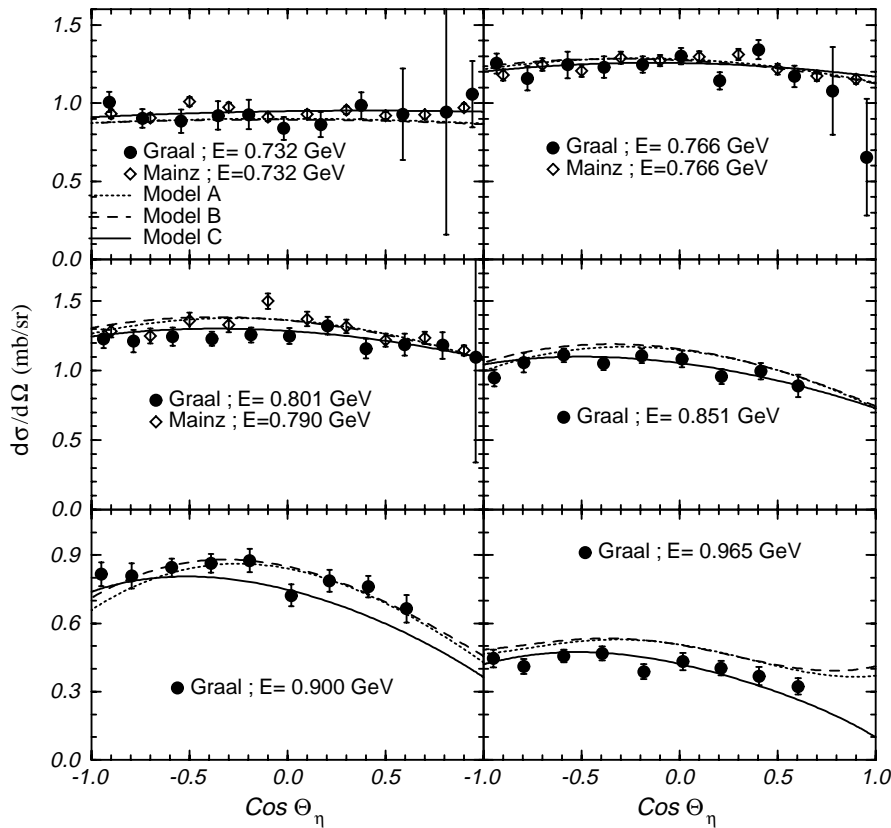
Fig. 1. Differential cross-section for the process $\gamma p \to \eta p$: angular distribution for $E_\gamma^{\text{lab}} = 0.732$ GeV to 0.965 GeV. The curves come from models A (dotted line), B (dashed line), and C (full line). Data are from refs. [20] (empty diamonds), and [23] (full circles).

dicted quark model value within the exact $SU(6) \otimes O(3)$ symmetry. Table 4 shows that these deviations stay indeed small for the $S_{11}(1650)$ and $D_{13}(1700)$. Compared to our previous work (see model M-7 in table 2 of ref. [27]), these coefficients decrease significantly due to a more copious data base. The rather large extracted strength value for the $D_{15}(1675)$ will be discussed later.

The new data set from Graal [23] included in the present work, brings in another change compared to our earlier work [27]: the width of the $S_{11}(1535)$ goes down from 230 MeV to about 140 MeV. This latter value, dictated by the higher-energy part of the Graal data, is compatible with the recent extractions from data [23,25]. The strong correlations among this quantity, the harmonic oscillator strength, the ηNN coupling, and the $S_{11}(1535)$ strength, explain the differences between the extracted values in ref. [27] and the present model A.

Finally, the mass of the $S_{11}(1535)$ comes out slightly smaller than its PDG value.

Model B: A correct treatment of the $SU(6) \otimes O(3)$ symmetry breaking requires the introduction of the mixing angles. We have used eqs. (16) to (19) to replace, as free parameters, the strengths of the $S_{11}(1535)$ and $S_{11}(1650)$ by θ_S and those of the $D_{13}(1520)$ and $D_{13}(1700)$ by θ_D. In table 4, we give in *italic* the values of those strengths using the extracted mixing angles and eqs. (16) to (19).

The absolute values of all four strengths decrease compared to those of model A. This is also the case for the resonance $D_{15}(1675)$. The other significant changes concern the strengths of the $P_{13}(1720)$ and $P_{11}(1710)$. This latter resonance plays, however, a minor role and hence its extracted strength bears large uncertainty. Note that the reduced χ^2 increases by about 15% compared to model A, because of the additional constraint on the configuration mixings.

Our extracted mixing angles are in agreement with the quark model predictions [49] and results coming from the large-N_c effective field theory based approaches [57, 58]. However, model B does not offer satisfactory features when compared to the data between threshold and 1.1 GeV (figs. 1 and 2).

Model C: Results of models A and B clearly show that an approach containing a correct treatment of the Born terms and including *all known resonances* in the s- and u-channels *does not* lead to an acceptable model, even within a broken $SU(6) \otimes O(3)$ symmetry scheme. The forward peaking behavior in the differential cross-section around 1.1 GeV suggests the presence of a large S-wave component that cannot be accommodated by the known S_{11} resonances.

To go further, one possible scenario is to investigate manifestations of yet undiscovered resonances, because of
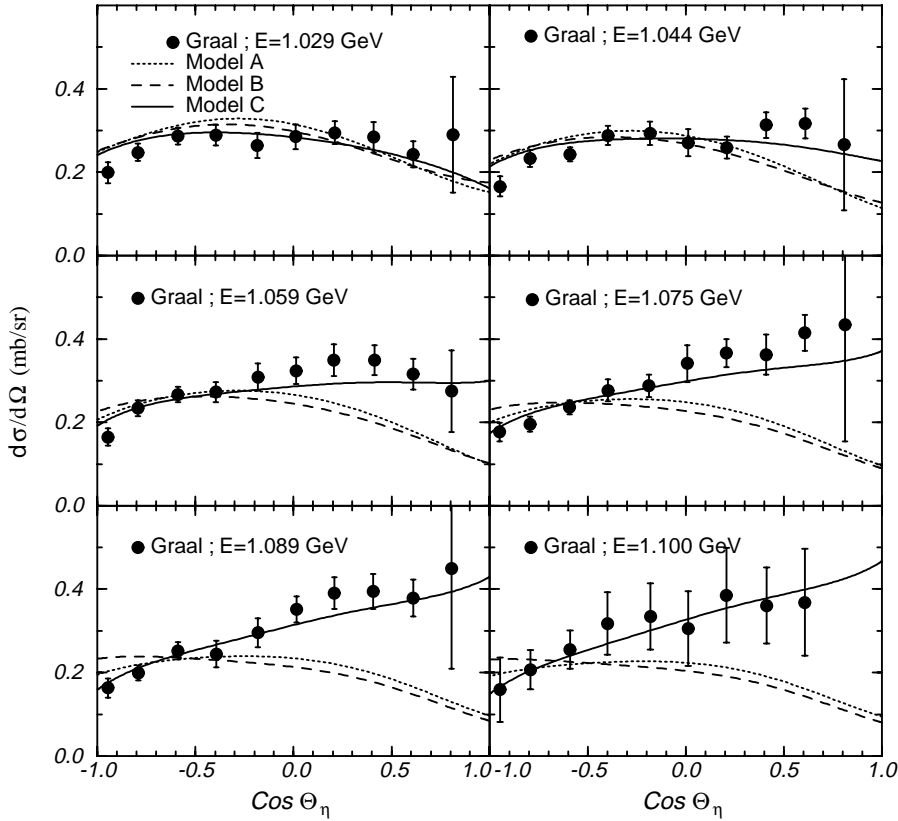
Fig. 2. Same as fig. 1, but for $E_\gamma^{\mathrm{lab}} = 1.029$ GeV to 1.1 GeV.

their weak or null coupling to the πN-channel. A rather large number of such resonances has been predicted by various authors. To find out which ones could be considered as relevant candidates, we performed a detail study of all the observables for which data are available and studied their multipole structures. This investigation, the results of which will be reported elsewhere, led us to the conclusion that a predicted [14] third S_{11} resonance, with $M = 1.712$ GeV and $\Gamma_T = 184$ MeV, could be an appropriate candidate. If there is indeed an additional S-wave resonance in this mass region, its dependence on incoming photon and outgoing meson momenta would be qualitatively similar to that of the $S_{11}(1535)$, even though the form factor might be very different. Thus, for this new resonance, we use the same CGLN amplitude expressions as for the $S_{11}(1535)$. We left, however, its mass and width, as well as its strength, as free parameters. The extracted values are given in table 4 and show amazingly close values to those predicted by the authors of ref. [14]. Moreover, for the one star $S_{11}(2090)$ resonance [6], the Zagreb group coupled-channel analysis [10] produces the following values: $M = 1.792 \pm 0.023$ GeV and $\Gamma_T = 360 \pm 49$ MeV.

The differential cross-sections are well reproduced (figs. 1 and 2) with this model. The reduced χ^2 is greatly improved and goes down to 1.6.

The strength of the harmonic oscillator α_{ho}^2 comes out the same for the three models and agrees with the findings of ref. [17].

Introducing this third resonance, hereafter referred to as $S_{11}(1730)$, modifies the extracted values for the parameters of the two other S_{11} resonances. The mass and width of the first S_{11} resonance come out compatible with their recent determination by the CLAS collaboration [25], as well as with those of the Zagreb group coupled-channel analysis [59].

Moreover, the strengths of the $P_{11}(1710)$, $P_{13}(1720)$, and $D_{15}(1675)$ get very close to their predicted values by the quark model based on the $SU(6) \otimes O(3)$ symmetry. The $F_{15}(1680)$ plays a non-negligible role and the two highest mass resonances, $P_{13}(1900)$ and $F_{15}(2000)$, have marginal contributions.

Finally, our extracted value for the ηNN coupling constant $g_{\eta NN}/\sqrt{4\pi} = 0.2$ is compatible with recent determinations [36,60] of this fundamental quantity. However, results from the RPI group [30] as well as from the hadronic sector [61] suggest values roughly between 2 and 7. Some possible origins of such discrepancies are discussed in the literature [62].

3.3 Total cross-section

Figure 3 shows the results for the total cross-section. These data *were not* included in the fitted data base. So, our curves can be considered as semi-predictions. Here, the most striking feature is a minimum around $W = 1.675$ GeV ($E_\gamma^{\mathrm{lab}} \approx 1.03$ GeV), also reported by
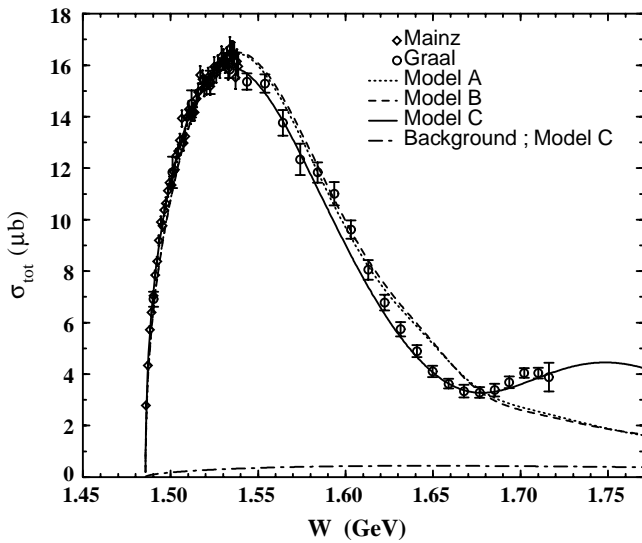
Fig. 3. Total cross-section for the reaction $\gamma p \to \eta p$ as a function of total center-of-mass energy. The dot-dashed curve comes from the background terms in model C, other curves and data are as in fig. 1.

the CLAS Collaboration [26] in the η electroproduction process.

Models A and B reproduce the data roughly up to $W = 1.62$ GeV, missing badly the higher-energy data. The introduction of the new resonance has a dramatic effect. The agreement between curve C and the data is reasonable, and especially the structure shown by data around $W = 1.7$ GeV is nicely reproduced. Note that, even the low-energy data are better reproduced by model C than by the two other models. Although the $S_{11}(1730)$ resonance has a too high mass to play a significant role close to threshold, its inclusion attributes to the other two S_{11} resonances more realistic roles. It is worthwhile noting that the background terms contribution (fig. 3) is small and bears no structure.

Another striking feature is that the inclusion of the new resonance leads to higher extracted values for both mass and width of the $S_{11}(1535)$ resonance, compatible with the partial-wave analysis [6,7] and a recent coupled-channel [59] results.

3.4 Polarization observables

There are two sets of data for single-polarization observables and we have investigated both.

Polarized beam asymmetry

The data come from the Graal collaboration [22] and contain 56 data points between 0.745 GeV and 1.09 GeV. In a previous work [27], we have performed a detailed study of these data published in 1998. Results of a more refined data analysis have been reported since then [24]. In the present work, we have hence included these latter data in
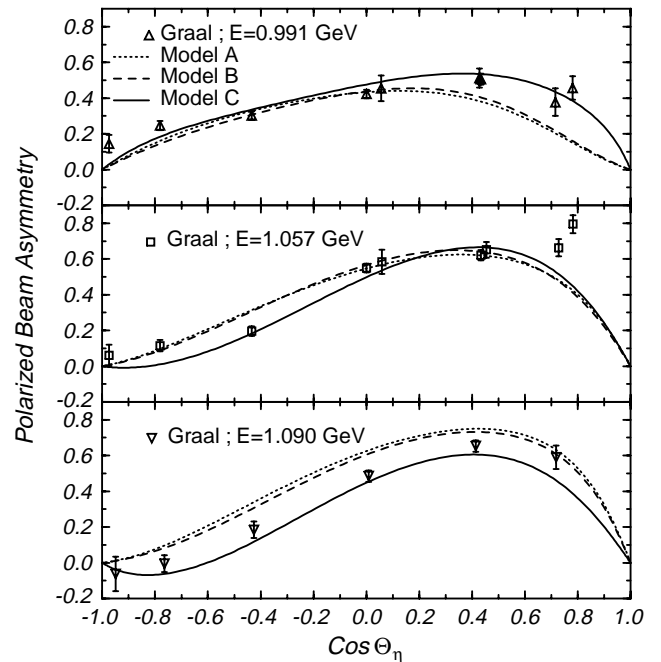

Fig. 4. Polarized beam asymmetry angular distributions for the reaction $\gamma p \to \eta p$. Curves are as in fig. 1, and data from refs. [22–24].

our fitted data base. A challenging problem concerns the data at 1.057 GeV: the two most forward angle data, at $\theta = 39°$ and to a less extent at $43°$, show an unexpected increase. In fig. 4, we show comparisons with data at this energy as well as at the two adjacent ones, where the forward angle data are better reproduced. Although we do not settle the problem raised by those two forward angle data points, we obtain a good description of the data, especially with model C.

For this observable, the quality of agreement with data at lower energies is comparable to that shown in fig. 4, and to limit the number of figures, we do not show them here.

Polarized target asymmetry

This observable has been measured at ELSA [21], between 0.717 GeV and 1.1 GeV at 7 energies corresponding to 50 data points.

To evaluate the predictive power of our approach, we *did not* include these data in our fitted data base. In fig. 5, the results are depicted at six measured energies with reasonable data points. In spite of the large experimental error bars, the superiority of model C in predicting this observable is obvious.

The nodal structure at low energies, seemingly indicated by the data, is however not reproduced. This feature has already been discussed in detail in a previous publication [27], and the conclusion presented there are not altered by the models presented in this work.
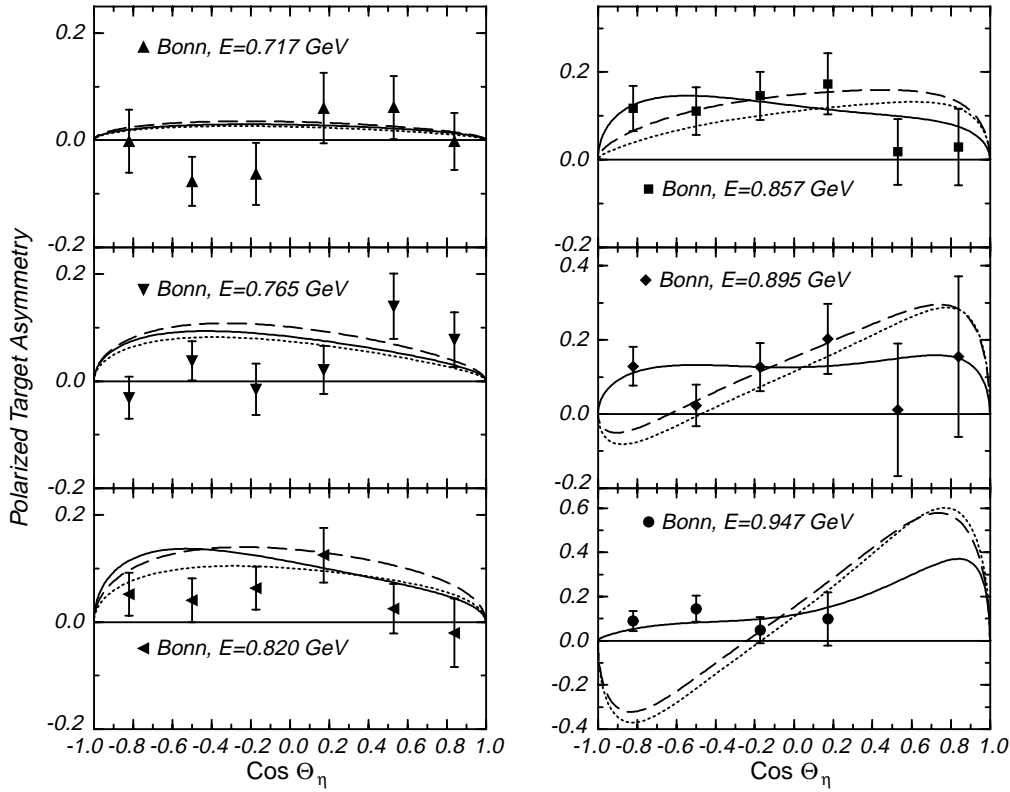
Fig. 5. Same as fig. 4, but for polarized target asymmetry. Curves are as in fig. 1, and data from ref. [21].

3.5 Photo-excitation helicity amplitudes and partial decay widths

The process under investigation offers the possibility of determining the electro-strong properties of the relevant baryons. The connection between such properties and QCD-based (or inspired) approaches has been emphasized by several authors [14,30,32,45].

Up to now, given the state of the art for both theory and experiment, the investigations have been basically focused on the $S_{11}(1535)$ resonance. In this section we discuss first the case of this resonance, then we introduce the relevant expressions for the $S_{11}(1650)$ resonance, before proceeding to other ones in the first and second resonance region.

For the $S_{11}(1535)$ resonance, the quantities of interest are the total width (Γ_T) of this latter resonance, and the electromagnetic helicity amplitude $A^p_{1/2}$. Moreover, $A^p_{1/2}$ can be related to the quantity ξ [31], characteristic of the photo-excitation of the $S_{11}(1535)$ resonance and its decay into the η-nucleon channel, by the following relation:

$$A^p_{1/2} = \sqrt{\frac{q}{k} \frac{M_R}{M_p} \frac{\Gamma_T}{b_\eta}}\, \xi \qquad (25)$$

and

$$\xi = \sqrt{\frac{\pi \alpha_\eta \alpha_e (E + M_p)}{M_R^3}} \frac{C_{S_{11}(1535)} \omega_\gamma}{6\Gamma_T}$$

$$\times \left[\frac{2\omega_\eta}{m_q} - \frac{2q^2}{3\alpha^2} \left(\frac{\omega_\eta}{E + M_p} + 1 \right) \right] \left(1 + \frac{k}{2m_q} \right) e^{-\frac{k^2+q^2}{6\alpha^2}}. \quad (26)$$

For the branching ratio $b_\eta \equiv \Gamma_{\eta N}/\Gamma_T$, we use 0.55 [6,25].

Given that the quark model used here predicts, in the $SU(6) \otimes O(3)$ symmetry limit, no contribution from the $S_{11}(1650)$ resonance, we cannot use the same approach as above for this latter resonance. However, we can derive the relevant expression for the partial width of this resonance following eqs. (21) and (22) in ref. [27]. This leads to the following relation where the Lorentz boost factor ($\mathcal{K}$ in table 2) has been explicitly incorporated:

$$\Gamma^{\text{exp}}_{S_{11}(1650)\to\eta N} = \pi\alpha \left[\alpha_{\eta NN} C^2_{S_{11}(1650)} \right]$$

$$\times \left[\frac{1}{(A^p_{1/2})^2} \right]^2 \left[\frac{2}{9} \frac{q}{k} \frac{M_N^3 E_\gamma^2}{M_{N^*}^2 E_f^2} \frac{s(E_f + M_N)}{(s + M_N^2)^2} \right]$$

$$\times \left[\frac{E_\eta}{m_q} - \frac{q^2}{3\alpha_{\text{ho}}^2} \left(\frac{E_\eta}{E_f + M_N} + 1 \right) \right]^2$$

$$\times \left(1 + \frac{k}{2m_q} \right)^2 e^{-\frac{k^2+q^2}{3\alpha_{\text{ho}}^2}}, \qquad (27)$$

with E_η the total energy of the outgoing η-meson.

For other resonances, we follow the expressions given in tables 2 and 3.

For the resonances considered in this paper, the quark model results for electromagnetic helicity amplitudes and the latest PDG values [6] are listed in tables 5 and 6.

Our results for the first two S_{11} resonances agree with the PDG values.

In the case of the $D_{13}(1520)$, both helicity amplitudes turn out compatible with those reported in the PDG. This is also the case for the $A^p_{1/2}$ components of the $D_{13}(1700)$, as well as for the $A^p_{3/2}$ component of the $F_{15}(1680)$ resonances.

For the other amplitudes reported in table 5, our results show significant deviations from the PDG values. Such trends are also reported in the literature [1,5,38,63–65].

In the case of the $D_{15}(1675)$, as mentioned above, we extract the helicity amplitudes for the photon-neutron coupling. Then, we determine those for the photon-proton coupling by using the following expressions [50]:

$$A^p_{3/2} \approx -0.31 A^n_{3/2}, \qquad (28)$$

and

$$A^p_{1/2} = (1/\sqrt{2}) A^p_{3/2}. \qquad (29)$$

Our results are given in table 6 and show good agreement with the PDG values for all four amplitudes.

The extraction of the ηN decay width is straightforward: the coefficients C_{N^*} for these resonances are given in table 4 and their masses and total decay widths in table 1. We present our numerical results for the partial widths and branching ratios of the relevant resonances in table 7, where the second column gives the predictions of the quark model (see table 3). The only uncertainty here comes from the coupling $\alpha_{\eta NN} \equiv 2g_{\eta NN} = 1.467 \pm 0.020$. The third column corresponds to $\Gamma^{\text{th}}_{\eta N} = C^2_{N^*} \Gamma^{\text{qm}}_{\eta N}$, where another source of uncertainty is introduced because of the coefficients C_{N^*}, as reported in table 4. In the fourth column our values for the experimental width $\Gamma^{\text{exp}}_{\eta N}$, as defined in eq. (24), are reported. For this quantity, the major origin of the uncertainties comes from those in the helicity amplitudes as given in the PDG (see table 5). In the last column of table 7, we give the branching ratio BR $= \Gamma^{\text{exp}}_{\eta N}/\Gamma_T$, where the total widths Γ_T are taken from the PDG (see last column in table 1). Our results for the $D_{13}(1520)$ are compatible with the width (0.6 MeV) reported in ref. [66], but the branching ratio is larger than the values given in ref. [28] (0.08 ± 0.01 and 0.05 ± 0.02). For the $F_{15}(1680)$ resonance the only other available value comes, to our knowledge, from an algebraic approach [18] which gives $\Gamma_{\eta N} = 0.5$ MeV, much smaller than our result.

The uncertainties of the helicity amplitudes $[A_{1/2}]_{\text{exp}}$ and $[A_{3/2}]_{\text{exp}}$, extracted from experiments and reported in the PDG [6], are the major constraints on the determination of the partial decay widths or branching ratios within the present approach. For resonances with large experimental helicity amplitudes, such as the resonances $D_{13}(1520)$ and $F_{15}(1680)$, the uncertainties are small, so

Table 5. Photo-excitation helicity amplitudes in units of 10^{-3} GeV$^{-1/2}$.

Resonance	$A^p_{1/2}$		$A^p_{3/2}$	
	Model C	PDG	Model C	PDG
$S_{11}(1535)$	64	90 ± 30		
$S_{11}(1650)$	52	53 ± 16		
$P_{11}(1710)$	-36	9 ± 22		
$P_{13}(1720)$	156	18 ± 30	-64	-19 ± 20
$D_{13}(1520)$	-9	-24 ± 9	149	166 ± 5
$D_{13}(1700)$	-21	-18 ± 13	146	-2 ± 24
$F_{15}(1680)$	34	-15 ± 6	124	133 ± 12

Table 6. Photo-excitation helicity amplitudes in units of 10^{-3} GeV$^{-1/2}$ for the $D_{15}(1675)$ resonance.

$A^n_{1/2}$		$A^n_{3/2}$		$A^p_{1/2}$		$A^p_{3/2}$	
Model C	PDG	Model C	PDG	Model C	PDG	Model C	PDG
-33	-43 ± 12	-46	-58 ± 13	10	19 ± 8	14	15 ± 9

Table 7. $N^* \to N\eta$ decay widths (in MeV) and branching ratios from model C.

Resonance	$\Gamma^{\text{qm}}_{\eta N}$	$\Gamma^{\text{th}}_{\eta N}$	$\Gamma^{\text{exp}}_{\eta N}$	BR$^{\text{exp}}$(%)
$S_{11}(1650)$			4.0 ± 0.1	1.8 ± 0.1
$D_{13}(1520)$	0.7 ± 0.1	0.6 ± 0.1	0.5 ± 0.2	0.4 ± 0.1
$F_{15}(1680)$	6.5 ± 0.1	29.1 ± 1.3	26.8 ± 9.4	20.6 ± 7.2

that the resulting errors in the ηN branching ratios are also small. The extracted values for these two resonances are in good agreement with those in the PDG, showing the consistency of our approach. However, for those resonances with smaller helicity amplitudes and larger uncertainties, such as the two P-wave resonances as well as the $D_{13}(1700)$ and the $D_{15}(1675)$, the ηN decay width could not be well determined within our approach. Moreover, the rather small coefficients C_{N^*} for these latter resonances obtained by fitting the photo-production data in our previous study are due to the fact that their electromagnetic couplings are small, which is indeed consistent with the quark model predictions. However, our results here show that the corresponding ηN decay widths for these resonances *could be large*.

The above considerations show clearly the need for more comprehensive measurement of the η photo-production for *both* proton and neutron targets. The latter is especially desirable in investigating the resonances $P_{11}(1710)$, $P_{13}(1700)$, $D_{13}(1700)$, and $D_{15}(1675)$, due to the fact that their electromagnetic couplings γn are larger than those for the proton target. Therefore, their contributions to the η photo-production could be very significant.

Finally, we would like to emphasize that the partial widths extracted via a coupled-channel T matrices

analysis [10] of the reactions $\pi N \rightarrow \eta N$ and $\eta N \rightarrow \eta N$ are $\Gamma_{S_{11}(1650) \rightarrow \eta N} = 13 \pm 7$ MeV, $\Gamma_{D_{13}(1520) \rightarrow \eta N} = 0.1 \pm 0.1$ MeV, and $\Gamma_{F_{15}(1680) \rightarrow \eta N} = 0.2 \pm 0.2$ MeV. Within the reported large uncertainties, the first two values are compatible with our findings, while the width of the $F_{15}(1680)$ is significantly smaller than our result.

4 Summary and conclusions

We reported here on a study of the process $\gamma p \rightarrow \eta p$ for E_γ^{lab} between threshold and ≈ 1.2 GeV, using a chiral constituent quark approach.

We extract the ηN branching ratio within our framework. The results for the $S_{11}(1650)$ and $D_{13}(1520)$ resonances are compatible with the existing data. For the resonance $F_{15}(1680)$, as our earlier investigation [27] showed, the strength of this resonance is very sensitive to the polarization observables. Thus, more accurate data in this area are needed to confirm if this resonance has a large ηN branching ratio, as found in this work.

We show how the symmetry breaking coefficients C_{N^*} are expressed in terms of the configuration mixings in the quark model, thus establish a direct connection between the photo-production data and the internal quark gluon structure of baryon resonances. The extracted configuration mixing angles for the S- and D-wave resonances in the second resonance region from a more complete data base are in good agreement with the Isgur-Karl model values [49], which predicted the configuration mixing angles based on the one-gluon exchange [50], as well as with results coming from the large-N_c effective field theory based approaches [57,58].

However, one of the common features in our investigation of the η photo-production at higher energies is that the existing S-wave resonance cannot accommodate the large S-wave component above $E_\gamma^{\text{lab}} \approx 1.0$ GeV region. Thus, we introduce a third S-wave resonance in the second resonance region suggested in the literature [14]. The introduction of this new resonance improves greatly the quality of our fit and reproduces very well the cross-section increase in the second resonance region. It even improves the agreement with low-energy data, by allowing the first region resonances to contribute in a more realistic way. In particular, it describes very well the forward peaking behavior compared to models A and B, without the third S-wave resonance, which fail to generate the same trend. The quality of our semi-prediction for the total cross-section and our predictions for the polarized target asymmetry, when compared to the data, gives confidence to the presence of a third S_{11} resonance, for which we extract some static and dynamical properties: $M \approx 1.730$ GeV, $\Gamma_T \approx 180$ MeV. These results are in very good agreement with those in ref. [14], and compatible with ones in ref. [59].

The dynamics of our models is partially based on the duality hypothesis[2], namely, the exclusion of the ρ and ω

---

[2] Strictly speaking, the duality is an exact mathematical tool which cannot be applied, without assumptions and approximations, to the real physical world [52]. According to this concept,

---

vector mesons exchange in the t-channel. However, our approach allows us to take into account individual contributions from all known nucleon resonances up to $F_{15}(2000)$, and treats as degenerate higher ones up to $G_{17}(2190)$. These facts seem to us a reasonable justification to apply that hypothesis. Actually, the manifestations of the duality in the case of pseudoscalar mesons have been discussed in detail in ref. [53]. In this latter study, it was shown that the t-channel exchanges mimic the *higher spin* resonances lacking in the models. In the present work, given the kinematics region under consideration, we do not expect significant contributions from resonances with spin and mass higher than those of the $G_{17}(2190)$ resonance. Moreover, the new resonance comes out to be an S_{11}-wave, while the contributions from higher spin and mass resonances, $P_{13}(1900)$ and $F_{15}(2000)$, are found marginal. More generally, in searching for new resonances, it is highly desirable to avoid t-channel contributions in order not to wash out possible manifestations of yet undiscovered resonances.

If the trend seen in the data from Graal is confirmed by higher-energy measurements, the existence of the new S_{11} resonance could be endorsed and this finding will have very important implications. Actually, this new resonance cannot be accommodated by the constituent quark model, which may suggests an exotic nature for this resonance, such as a ΣK or ΛK type molecule [14]. If this is indeed the case, the investigation of this resonance in other reactions might be certainly warranted to understand its internal structure. For example, a systematic study of the kaon photo-production in the threshold region in different isospin channels would certainly shed some light on this resonance. The η and kaon electroproduction will also be very desirable to study the Q^2-dependence [70] of transition amplitudes. The QCD counting rule implies different Q^2-dependence for resonances with a three-quark constituent or other types of internal structure.

Certainly, forthcoming data from existing facilities will provide us with more information on the existence and the nature of this resonance.

Note: after the submission of this manuscript, the BES Collaboration reported [71] on the measurements of the

---

at any energy one could use *either* the s-channel resonance prescription *or* the t-channel Regge pole description, provided that we sum over an *infinite* number of terms. An approximation to this idea and widely discussed in the literature [52], is to express the physical scattering as a series of s-channel resonances plus a general background. In the present work, we have adopted this approximation. In other studies on the process investigated here *but* limited to the first resonance region, both s- and t-channel terms have been introduced (see *e.g.*, refs. [30–34]), based on the "interference model" [67] approxiamtion. However, it is known [68,69] that including a combination of s- and t-channel in a dynamical model leads to severe problems of double counting. Close to threshold, since the reaction mechanism is dominated by the $S_{11}(1530)$ and $D_{13}(1520)$ resonances, adding on top of these two s-channel resonances, contributions from t-channel might still be safe. In our case, given that we include all known N^* resonances, adding t-channel contributions would lead to real double counting troubles.

$J/\psi \to p\overline{p}\eta$ decay channel. A partial-wave analysis leads to the extraction of the mass and width of the $S_{11}(1535)$ and $S_{11}(1650)$ resonances. Moreover, the authors find indications for a third S_{11} resonance, $J^P = 1/2^+$, with $M = 1.800 \pm 0.040$ GeV, and $\Gamma_T = 165^{+165}_{-85}$ MeV.

References

1. S. Capstick, W. Roberts, Prog. Part. Nucl. Phys., **45** (Suppl. 2), 5241 (2000).
2. R. Bijker, F. Iachello, A. Leviatan, Ann. Phys. **236**, 69 (1994); **284**, 89 (2000).
3. L.Ya. Glozman, D.O. Riska, Phys. Rep. **268**, 263 (1996).
4. M. Anselmino, E. Predazzi, S. Ekelin, S. Fredriksson, D.B. Lichtenberg, Rev. Mod. Phys. **65**, 1199 (1993).
5. S. Capstick, Phys. Rev. D **46**, 2864 (1992); S. Capstick, W. Roberts, Phys. Rev. D **49**, 4570 (1994).
6. Particle Data Group, Eur. Phys. J. **15**, 1 (2000).
7. D.M. Manley, E.M. Saleski, Phys. Rev. D **45**, 4002 (1992).
8. T.P. Vrana, S.A. Dytman, T.S.H. Lee, Phys. Rep, **328**, 181 (2000).
9. J.C. Nacher, A. Parreno , E. Oset, A. Ramos, A. Hosaka, M. Oka, Nucl. Phys. A **678**, 187 (2000).
10. M. Batinić, I. Dadič, I. Šlaus, A. Švarc, B.M.K. Nefkens, T.S.H. Lee, Phys. Scr. **58**, 15 (1998).
11. N. Kaiser, P. Siegel, W. Weise, Phys. Lett. B **362**, 23 (1995).
12. C. Deutsch-Sauermann, B. Friman, W. Noerenberg, Phys. Lett. B **341**, 261 (1995).
13. L.Ya. Glozman, D.O. Riska, Phys. Lett. B **366**, 305 (1996).
14. Z. Li, R. Workman, Phys. Rev. C **53**, R549 (1996).
15. R. Koniuk, N. Isgur, Phys. Rev. D **21**, 1868 (1980).
16. S. Capstick, N. Isgur, Phys. Rev. D **34**, 2809 (1986).
17. Z. Li, F.E. Close, Phys. Rev. D **42**, 2207 (1990).
18. R. Bijker, F. Iachello, A. Leviatan, Phys. Rev. C **54**, 1935 (1996).
19. S.A. Dytman *et al.*, Phys. Rev. C **51**, 2710 (1995); J.W. Price *et al.*, Phys. Rev. C **51**, R2283 (1995).
20. B. Krusche *et al.*, Phys. Rev. Lett. **74**, 3736 (1995).
21. A. Bock *et al.*, Phys. Rev. Lett. **81**, 534 (1998).
22. J. Ajaka *et al.*, Phys. Rev. Lett. **81**, 1797 (1998).
23. F. Renard *et al.*, submitted to Phys. Rev. Lett., hep-ex/0011098.
24. F. Renard, PhD Thesis, University of Grenoble, 1999 (in French).
25. D. Armstrong *et al.*, Phys. Rev. D **60**, 052004 (1999).
26. R. Thompson *et al.*, Phys. Rev. Lett. **86**, 1702 (2001).
27. Z. Li, B. Saghai, Nucl. Phys. A **644**, 345 (1998).
28. L. Tiator, D. Drechsel, G. Knöchlein, C. Bennhold, Phys. Rev. C **60**, 035210 (1999).
29. G. Knoechlein, D. Drechsel, L. Tiator, Z. Phys. A **352**, 327 (1995).
30. N.C. Mukhopadhyay, J. F. Zhang, M. Benmerrouche, Phys. Lett. B **3**, 1 (1995).
31. M. Benmerrouche, N.C. Mukhopadhyay, J. F. Zhang, Phys. Rev. D **51**, 3237 (1995).
32. B. Krusche, N.C. Mukhopadhyay, J. F. Zhang, and M. Benmerrouche, Phys. Lett. B **397**, 171 (1997).
33. N.C. Mukhopadhyay, N. Mathur, Phys. Lett. B **444**, 7 (1998).
34. R.M. Davidson, N. Mathur, N.C. Mukhopadhyay, Phys. Rev. C **62**, 058201 (2000).
35. L. Chen, H.-C. Chiang, Phys. Lett. B **329**, 424 (1994).
36. L. Tiator, C. Bennhold, S.S. Kamalov, Nucl. Phys. A **580**, 455 (1994).
37. J. Denschlag, L. Tiator, D. Drechsel, Eur. Phys. J. A **3**, 171 (1998).
38. T. Feuster, U. Mosel, Phys. Rev. C **59**, 460 (1999).
39. A.M. Green, S. Wycech, Phys. Rev. C **60**, 035208 (1999).
40. C. Deutsch-Sauermann, B. Friman, W. Noerenberg, Phys. Lett. B **409**, 51 (1997).
41. C. Bennhold, H. Tanabe, Nucl. Phys. A **530**, 625 (1991).
42. N. Kaiser, T. Waas, W. Weise, Nucl. Phys. A **612**, 297 (1997).
43. J. Caro Ramon, N. Kaiser, S. Wetzel, W. Weise, Nucl. Phys. A **672**, 249 (2000).
44. B. Borasoy, Eur. Phys. J. A **9**, 95 (2000).
45. Z. Li, Phys. Rev. C **52**, 1648 (1995).
46. Z. Li, H. Ye, M. Lu, Phys. Rev. C **56**, 1099 (1997).
47. Q. Zhao, B. Saghai, Z. Li, submitted to Phys. Rev. C, nucl-th/0011069.
48. R.H. Stanley, H.J. Weber Phys. Rev. C **52**, 435 (1995).
49. N. Isgur, G. Karl, Phys. Lett. B **72**, 109 (1977).
50. N. Isgur, G. Karl, R. Koniuk, Phys. Rev. Lett. **41**, 1269 (1978).
51. A. Manohar, H. Georgi, Nucl. Phys. B **234**, 189 (1984).
52. See, *e.g.,* P.D.B. Collins, Phys. Rep. **1**, 103 (1971); V. Alessandrini *et al.*, Phys. Rep. **1**, 269 (1971); F.J. Gilman, Phys. Rep. **4**, 95 (1972); J.H. Schwarz, Phys. Rep. **8**, 269 (1973); G. Veneziano, Phys. Rep. **9**, 199 (1974); P.H. Frampton, *Dual Resonance Models* (W.A. Benjamin Inc., 1974); P. Collins, *An Introduction to Regge Theory and High Energy Physics* (Cambridge University Press, 1977).
53. B. Saghai, F. Tabakin, Phys. Rev. C **53**, 66 (1996); Phys. Rev. C **55**, 917 (1997); B. Saghai, nucl-th/0105001.
54. Z. Li, Phys. Rev. D **48**, 3070 (1993); Phys. Rev. D **50**, 5639 (1994).
55. R. G. Moorhouse, Phys. Rev. Lett. **16**, 772 (1966).
56. F. James, M. Roos, Comput. Phys. Commun. **10**, 343 (1975).
57. C.D. Carone, H. Georgi, L. Kaplan, D. Morin, Phys. Rev. D **50**, 5793 (1994); C.E. Carlson, C.D. Carone, Phys. Rev. D **58**, 053005 (1998); C.E. Carlson, C.D. Carone, J.L. Goity, R.F. Lebed, Phys. Lett. B **438**, 327 (1998); C.E. Carlson, C.D. Carone, J.L. Goity, R.F. Lebed, Phys. Rev. D **59**, 114008 (1999).
58. D. Pirjol, T.-M. Yan, Phys. Rev. D **57**, 1449 (1998); Phys. Rev. D **57**, 5434 (1998).
59. A. Švarc, S. Ceci, nucl-th/0009024.
60. C. Bennhold, L. Tiator, S.S. Kamalov, Nucl. Phys. A **585**, 313c (1995).
61. K. Holinde, Nucl. Phys. A **543**, 143c (1992); J. Piekarewicz, Phys. Rev. C **48**, 1993 (1993); T. Feuster, U. Mosel, Phys. Rev. C **58**, 457 (1998); E. Gedalin, A. Moalem, L. Razdolskaja, Nucl. Phys. A **634**, 368 (1998).

62. M. Kirchbach, L. Tiator, Nucl. Phys. A **604**, 385 (1996); S. Neumeier, M. Kirchbach, hep-ph/9809246; M. Kirchbach, Int. J. Mod. Phys. A **15**, 1435 (2000); Phys. Lett. B **455**, 259 (1999); A. L. L'vov, A. M. Nathan, Phys. Rev. C **59**, 1064 (1999).

63. R.A. Arndt, I.I. Strakovsky, R.L. Workman, M.M. Paven, Phys. Rev. C **52**, 2120 (1995); R.A. Arndt, I.I. Strakovsky, R.L. Workman, Phys. Rev. C **53**, 430 (1996).

64. E. Perazzi, M. Radici, S. Boffi, Nucl. Phys. A **614**, 346 (1997).

65. D. Drechsel, O. Hanstein, S.S. Kamalov, L. Tiator, Nucl. Phys. A **645**, 145 (1999).

66. R. Bijker, F. Iachello, A. Leviatan, Phys. Rev. D **55**, 2862 (1997).

67. V. Barger, M. Olsson, Phys. Rev. **151**, 1123 (1966);5 V. Barger, D. Cline, Phys. Rev. Lett. **16**, 913 (1966); Phys. Rev. **155**, 1792 (1967).

68. R. Dolen, D. Horn, C. Schmid, Phys. Rev. **166**, 1768 (1968).

69. G.F. Chew, A. Pignotti, Phys. Rev. Lett. **20**, 1078 (1968).

70. C.E. Carlson, N.C. Mukhopadhyay, Phys. Rev. D **41**, 2343 (1990); Phys. Rev. Lett. **67**, 3745 (1991); Phys. Rev. D **47**, R1737 (1993); Phys. Rev D **58**, 094029 (1998); C.E. Carlson, *Proceeding of the NSTAR 2000 Conference on Excited Nucleons and Hadronic Structure Newport News (USA), 16–19 Feb. 2000*, edited by V.D. Burkert, L. Elouadrhiri, J.J. Kelly, R.C. Minehart (World Scientific, 2001).

71. J.Z. Bai *et al.*, hep-ex/0105011.